

## **Support information**

### **Interface Regulation Promoting Carbon Monoxide Gas Diffusion Electrolysis towards C<sub>2+</sub> Products**

*Yingzhang Yan,<sup>a</sup> Yonghao Yu,<sup>b</sup> Yumin Zhang,<sup>\*c</sup> Tai Yao,<sup>\*c</sup> Ping Xu,<sup>d</sup> and Bo Song<sup>\*a,c</sup>*

- a School of Physics, Harbin Institute of Technology, Harbin 150001, China.*
- b HIT Center for Analysis, Measurement and Computing , Harbin Institute of Technology, Harbin 150001,China*
- c National Key Laboratory of Science and Technology on Advanced Composites in Special Environments, Harbin Institute of Technology, Harbin 150001, China. E-mail address: [songbo@hit.edu.cn](mailto:songbo@hit.edu.cn) , [zhym@hit.edu.cn](mailto:zhym@hit.edu.cn), [yaotai@hit.edu.cn](mailto:yaotai@hit.edu.cn).*
- d School of Chemistry and Chemical Engineering, Harbin Institute of Technology, Harbin 150001, China.*

### *Electrode fabrication*

*Materials and Chemicals:* Commercial copper nanoparticle (average particle diameter of 25 nm) was purchased from Sigma-Aldrich. Polymethyl methacrylate (PMMA) was purchased from Arkema. Conductive carbon Ketjen black (ECP600JD) was purchased from LION (Japan). Copper target (99.995%) was purchased from ZhongNuo Advance Material (Beijing) Technology Co., Ltd. Dimethyl Formamide (DMF) was purchased from Macklin, and isopropanol was purchased from Tianji Fuyu Fine chemical corporation. Carbon-based gas diffusion layer (Sigracet 28 BC) was purchased from Fuel Cell Store, high purity N<sub>2</sub> (99.999%) and CO (99.99%) were purchased from Liming Gas Group.

*Synthesis of Cu@PMMA-MS, Cu@PMMA-MS/C, MS-500, commercial Cu on gas diffusion layer.*

Cu@PMMA-MS were fabricated using the electro-spray method followed by magnetic sputtering. For the typical process, PMMA solutions with concentrations of 4%, 6%, 8%, 10%, 12% and 15% were prepared by dissolving 100 mg PMMA powder in 2.4, 1.775, 1.15, 0.9, 0.733 and 0.567 g DMF, respectively with continuous string for 12 h. Then, 100 mg commercial Cu and 10 mg Ketjen black were evenly distributed in PMMA solutions to form spinning dispersions. The gas diffusion layer was cut into 2 cm in square, serving as the substrate. Dispersion was then transferred into a syringe, which was fixed on an automatic injection pump. During the spinning process, relevant temperature and humidity were fixed at  $23 \pm 2^\circ\text{C}$  and  $40 \pm 5\%$ . Dispersion would be continuously transported to the tip of the needle with a feeding rate of  $0.2 \text{ mL h}^{-1}$ . A fixed voltage of 12 kV was applied between the needle and the substrate through a high voltage DC power. The dispersion was sprayed onto the substrate with a work distance of 15 cm. Subsequently, magnetron sputtering was carried out in Ar with an RF power of 100 W after the chamber was pumped down below  $10^{-5}$  Torr, the sputtering duration was optimized to be 500 s.

Cu@PMMA-MS/C was fabricated by spray coating a mixture of Ketjen black and Nafion solution onto the Cu@PMMA-MS: 1 mg Ketjen Black and 10  $\mu\text{L}$  5wt % Nafion solution was dispersing in 1 mL isopropanol through ultrasonication. During the spray-coating process, the substrates were maintained at  $70^\circ\text{C}$  using a hot plate.

MS-500 was fabricated by magnetron sputtering of Cu on GDL substrate for 500 s.

Commercial Cu coated GDL was fabricated by spray-coating a homogenous ink composed of 5 mg commercial Cu, 50  $\mu\text{L}$  5wt % Nafion solution, 1.5 mL isopropanol and 0.5 mL deionized water ( $18.2 \text{ M}\Omega\cdot\text{cm}$ ), during the spray-coating process, the substrate was maintained at  $70^\circ\text{C}$ . Unless special declared, commercial Cu was abbreviated as Cu in the manuscript.

### *Flow cell electrolyzer Configuration assembly and operation*

The homemade flow cell comprises three chambers holding anolyte, catholyte and gas, respectively. The anolyte chamber (dimensions: 25 mm  $\times$  25 mm; 15 mm depth) contains a counter electrode (nickel foam, 1.6 mm thickness). The catholyte chamber (dimensions: 25 mm  $\times$  25 mm; 15 mm depth, square through-hole) contains a Hg/HgO reference electrode via a port drilled through the housing such that the reference electrode is in the centre of the chamber. An anion exchange membrane separates the anolyte and catholyte chambers (Fumasep FAB-PK-130). The snake-shaped gas flow channel (dimensions: 24.5 mm  $\times$  24.5 mm; 5 mm depth, 0.5 mm width) is used to supply the reactant gas. The gas and catholyte chambers are separated by the cathode. The catalyst side of the cathode faces into the catholyte chamber, while the gas

diffusion layer faces the gas chamber. Fluororubber gaskets with a window were placed between layers to achieve sufficient sealing. Each chamber has an inlet and outlet connection to flow either electrolyte or gas. Designed cathodes and Ni foam anodes were mounted in their respective chambers. Building up from the anolyte chamber, the completed assembly was sealed with even compression from four equally spaced bolts. The cathode was operated as the working electrode.

### Electrochemical Measurements

All the electrochemical tests mentioned were carried out using an electrochemical workstation (CHI 660E). Without specific clarification, the used electrolyte was 1 M KOH. The ECOR performance was tested in a flow cell assembly under galvanostatic mode. Cu@PMMA-MS, Cu@PMMA-MS/C and commercial Cu were used as the cathodes in different tests. CO was supplied to the gas chamber of the flow cell with a constant flow rate of 15 sccm, controlled by a digital mass flow controller (Aserit). All potentials were converted to reversible hydrogen electrode (RHE) scale via the equation:

$$E_{RHE} = E_{Hg/HgO} + 0.098V + 0.059 \times pH + iR$$

where R is the overall ohmic resistance (including electrolytes and membrane) of the cell was measured by EIS,  $E_{RHE}$  is the potential of RHE,  $E_{Hg/HgO}$  is the applied potential, and  $pH$  is the basicity of the catholyte.

Unless otherwise stated, the volumes of catholyte and anolyte used for circulation were 25 mL, electrolytes were supplied to the cell at a constant flow rate of 10 ml·min<sup>-1</sup> through peristaltic pumps through PTFE tubing. The liquid products were collected after 2 hours of continuous operation for analysis. The current densities reported were normalized by the geometric surface area.

ECSA Methods: Cyclic Voltammetry (CV) scans were recorded at five scan rates with a minimum of 3 cycles in the non-Faradaic region, specifically between -0.075 V vs. RHE and 0.125 V vs. RHE. Scan rates of 20 mV/s, 40 mV/s, 60 mV/s, 80 mV/s, and 100 mV/s were used. The difference between currents at 0.025 V vs. RHE was plotted against the scan rate to extract the slope. The half slope of this line corresponds to the capacitance of the catalyst's electric double layer in Farads. The electrochemical surface area (ECSA) can be determined by comparing the electric double layer capacitance to that of a perfectly flat copper, which was measured under constant CO flow and the recirculation of 1 M KOH electrolyte.

### Products Analysis

The gas products from CO reduction (H<sub>2</sub>, CH<sub>4</sub> and C<sub>2</sub>H<sub>4</sub>) were analyzed using a gas chromatograph (Agilent 7820A) coupled with a thermal conductivity detector (TCD) and a flame ionization detector (FID). The gas chromatograph was equipped with a Molecular Sieve 5A and HP-PLOT Al<sub>2</sub>O<sub>3</sub> columns. High purity N<sub>2</sub> was used as the carrier gas. All Faradaic efficiencies reported were averaged from at least three different runs. The Faradaic Efficiencies (FEs) were determined as a function of operating current, gas chromatography and flow rate at the outlet of the gas chamber as:

$$FE = n \cdot F \cdot \theta \cdot f_m / J$$

Where n is the number of electrons for a given product; F is the Faradaic constant;  $\theta$  is the volume fraction of the gases;  $f_m$  is the molar reacting gas flow rate; J is the current.

Liquid product analysis: Liquid products were analyzed via nuclear magnetic resonance spectroscopy (NMR) from respective catholyte solutions. A new cathode, catholyte, and

analyte were used for the collection of a single liquid product distribution at a given applied potential. A constant volume of 25 ml was recirculated through anode and cathode compartments using peristaltic pumps. The flow cell was operated at the desired applied potential for 7200 s. Cathode electrolyte was collected from the flow cell and tubing, sealed and stored in a fridge until NMR sample preparation. For NMR sample preparation, 0.5 mL stored solutions were mixed with 0.1 mL D<sub>2</sub>O and 0.02  $\mu$ L DMSO (internal standard) in NMR tubes. <sup>1</sup>H NMR spectra were collected on Bruker AVANCE III 600M in D<sub>2</sub>O in water suppression mode, and liquid product distributions were obtained by analyzing the resulting spectra in MestReNova.

#### *Characterization*

SEM were conducted on a Hitachi SU8020 field emission SEM. The accelerating voltage for SEM is 10 kV, respectively. Transmission electron spectroscopy images (TEM) and elemental mappings (EDS) were collected using a JEM-2100F microscope equipped with an Oxford energy-dispersive X-ray analysis system, with the accelerating voltage of 200 kV. PXRD was performed on a Rigaku D/max 2500 X-ray diffractometer using Cu K $\alpha$  radiation. XPS was performed on an ESCALAB KII spectrometer with an Al K $\alpha$  excitation source.

#### *In situ Raman analysis*

In-situ Raman test during electrochemical reduction. The in-situ Raman tests were conducted in a three-electrode spectro-electrochemical flow cell as shown in Figure S9 The obtained GDE was used as working electrode, a Pt wire as the counter electrode, and a saturated Ag/AgCl as the reference electrode. The anode and cathode compartments were separated by an anion exchange membrane (Fumasep FAB-PK-130) to avoid cross-contamination. During the tests, CO gas was flowing from the back side of the GDE to avoid the interfere with Raman signal. Electrolyte solutions were supplied to the cell at a constant flow rate of 10 ml·min<sup>-1</sup> through peristaltic pumps through PTFE tubing. The electrochemical tests were conducted using an electrochemical workstation (CHI 660E). The Raman tests were performed on a LabRAM HR Evolution microscope (inVia-Reflex) equipped with a 785 nm laser<sup>1</sup>, a 50 X objective, a monochromator (600 grooves/mm grating), and a CCD detector. Signal acquisition time for each Raman spectrum is about 60 seconds.

#### *Finite element analysis for reaction process modeling*

Multi species transport within the gas diffusion layer (GDL) were modeled in COMSOL 5.4 (Cells and Fuel cells module). The geometry modeled a steady state two-dimensional domain shown in Figure S20 with a GDL, catalyst layer (CL), and electrolyte sub-domains, the middle of the GDL is slightly recessed due to the compression from the wall of flow channel. The model uses current balances, mass transport equations (Maxwell-Stefan diffusion for reactants, CO and N<sub>2</sub>), and momentum transport (Darcy's law for the gas flows) to simulate the flow cell's behavior. For model simplification, C<sub>2</sub>H<sub>4</sub> was chose as the only product. The cathode C<sub>2</sub>H<sub>4</sub> current density and the local concentration of reactant were monitored.

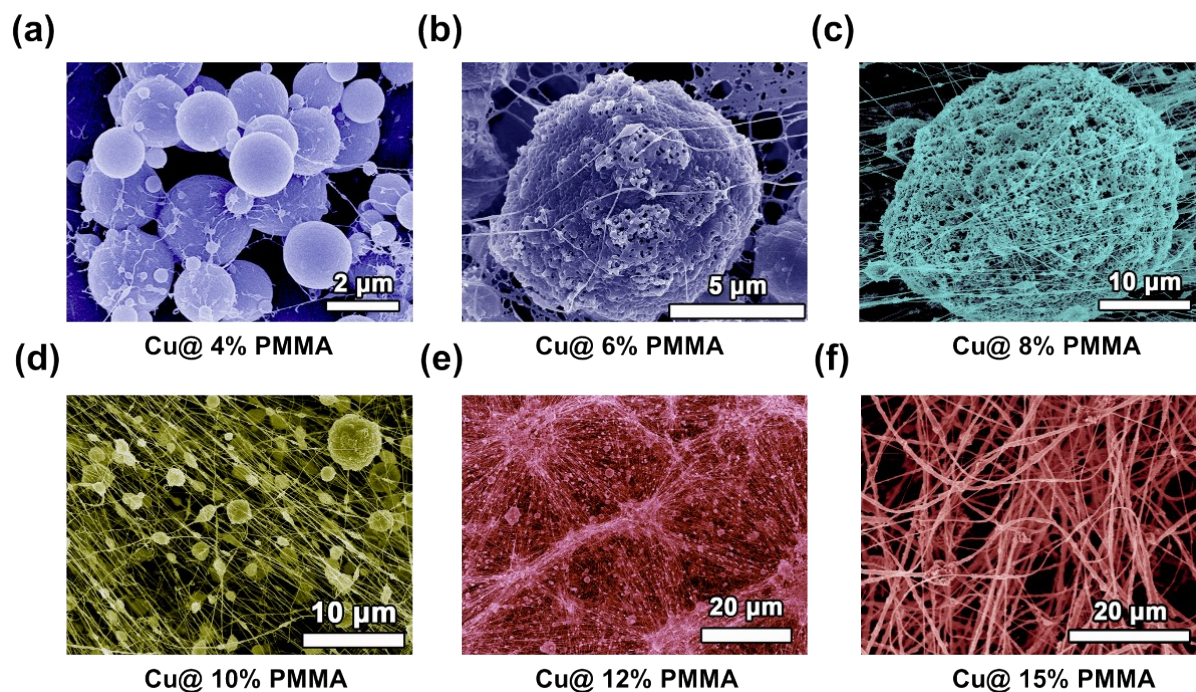


**Figure S1.** SEM images of as-synthesized Cu@X% PMMA as a function of PMMA concentration in DMF solution.

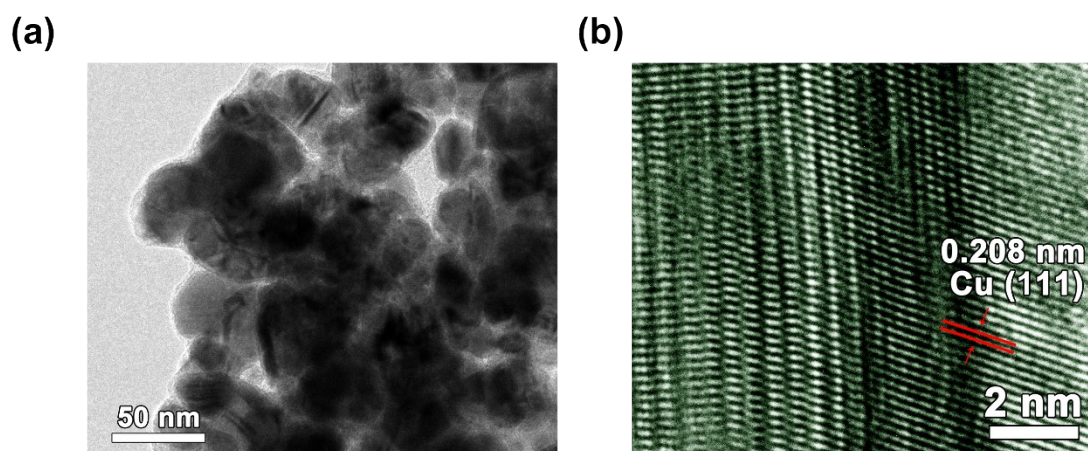
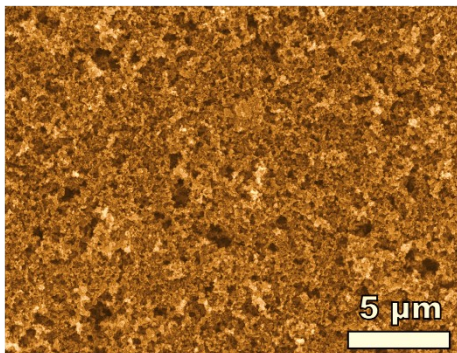


**Figure S2.** Catalyst used was commercial Cu nanoparticles without any further chemical modification. a) transmission electron microscopy (TEM) image shows that the average size of Cu nanoparticles is  $\sim 25$  nm.; and b) High resolution TEM (HRTEM) image clearly shows the lattice fringe refers to Cu (111) crystal face.

(a)



(b)

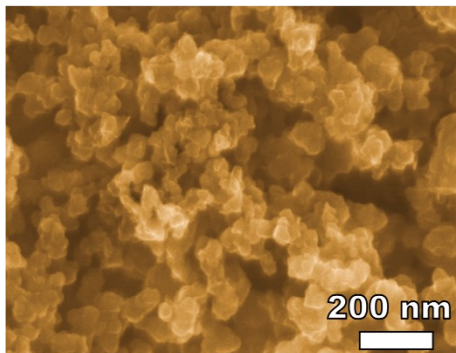


**Figure S3.** SEM images of Ketjen black in different magnification scales.

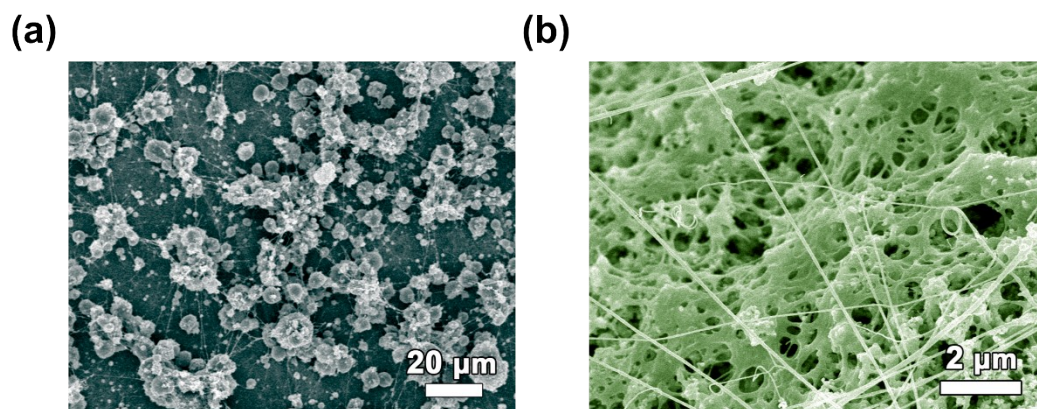


**Figure S4.** SEM images of Cu@8% PMMA in different magnification scales. The scale bars are a) 20 μm, and b) 2 μm, respectively. Cu@ 8%PMMA exhibits a transition state between sphere and nanofibers. Its shape possesses the structural merits from both nanofiber and sphere. The whole structure is rich in gas channel, which is beneficial for the gas transportation.

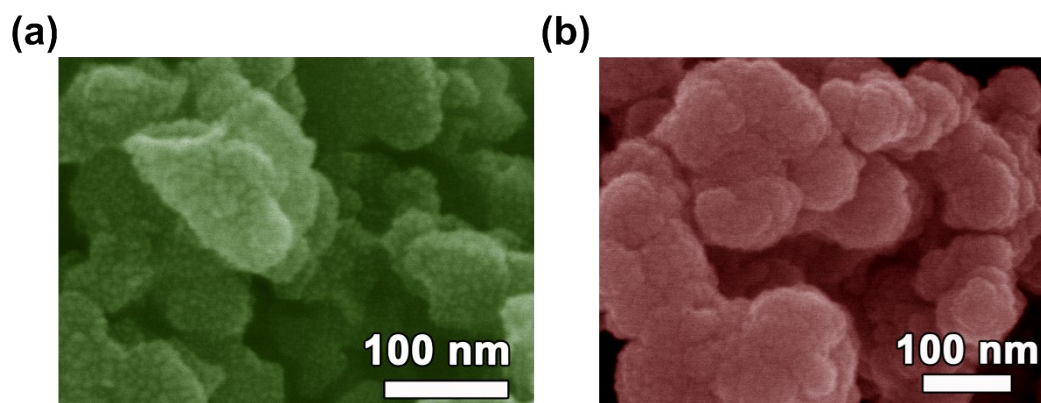


**Figure S5.** Cu deposition onto the surface of Cu@ 8%PMMA via magnetron sputter (MS) with a deposition rate of  $\sim 1 \text{ \AA s}^{-1}$ . a) MS 30s with deposited nanoparticle size of  $\sim 3 \text{ nm}$  b) MS 500 s with deposited layer of  $\sim 50 \text{ nm}$ .

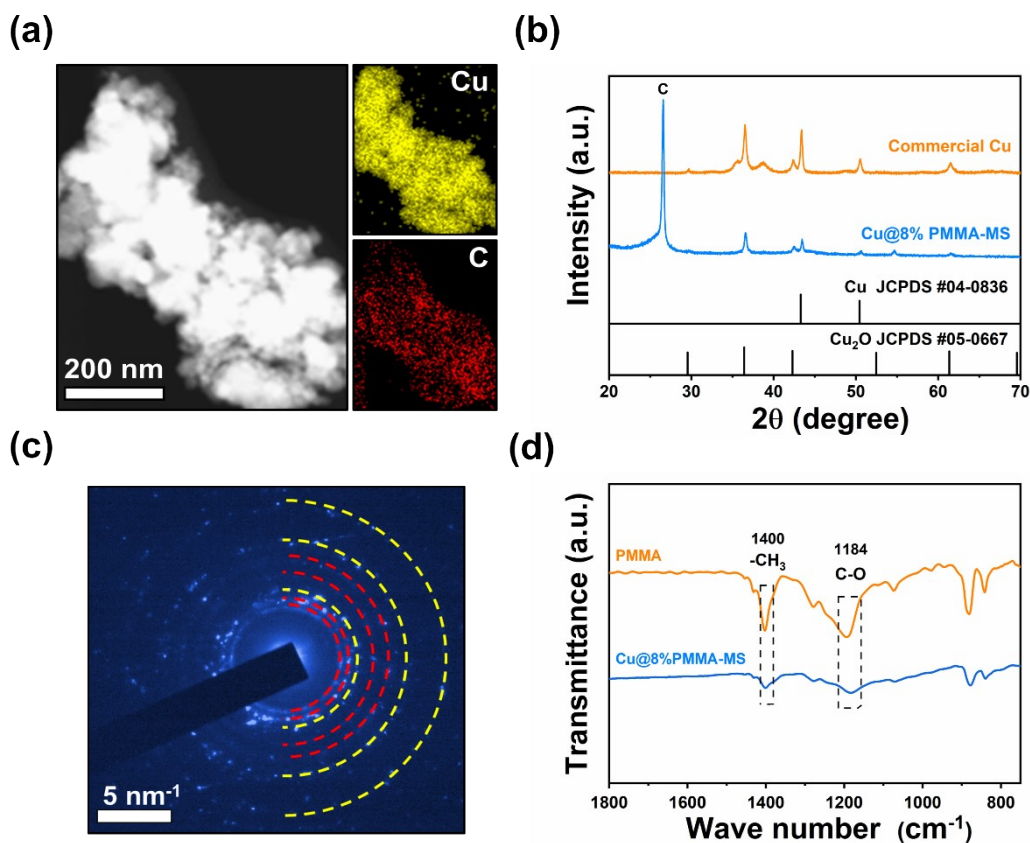


**Figure S6.** Structural characterizations of Cu@8% PMMA nanostructures. a) Dark-field TEM image and the corresponding elemental mappings of Cu and C in Cu@8% PMMA. b) PXRD patterns of the samples in comparison with the standard PXRD patterns of Cu (JCPDS 04-0836) and Cu<sub>2</sub>O (JCPDS 05-0667). c) SAED pattern for Cu@8%PMMA-MS. d) FTIR spectra of PMMA powder and Cu@8%PMMA-MS.

Energy dispersive X-ray spectroscopy (EDS) mapping analysis in Figure S6a confirms the evenly distribution of Cu and C elements, demonstrating the uniform mixture of commercial copper and KB. High resolution powder X-ray diffraction (PXRD) patterns (Figure S6b) confirmed the existence of both metallic Cu, and trace impurities of Cu<sub>2</sub>O in all samples, probably due to the exposure to air<sup>2,3</sup>. Further, the diffraction peak located at  $2\theta$  value of  $26.5^\circ$  distinctly indicates the (200) plane of carbon. Selected area electron diffraction (SAED) patterns (Figure S6c) reveal the polycrystalline nature of Cu@8% PMMA-MS. The inner to outer diffraction rings in yellow can be indexed to (111), (220), (400) planes of Cu (JCPDS 04-0836), and the diffraction rings in red can be indexed to Cu<sub>2</sub>O (JCPDS 05-0667), respectively, well consistent with PXRD patterns. To further probe the structural information, the Fourier transform infrared spectroscopy (FTIR) measurement was performed (Figure S6d). The peaks located at  $\sim 1184\text{ cm}^{-1}$  and  $\sim 1400\text{ cm}^{-1}$ , which was assigned to stretch model of  $-\text{OCH}_3$  and  $-\text{CO}$ , respectively<sup>4</sup>, convincingly demonstrated the existence of PMMA in Cu@8% PMMA-MS.

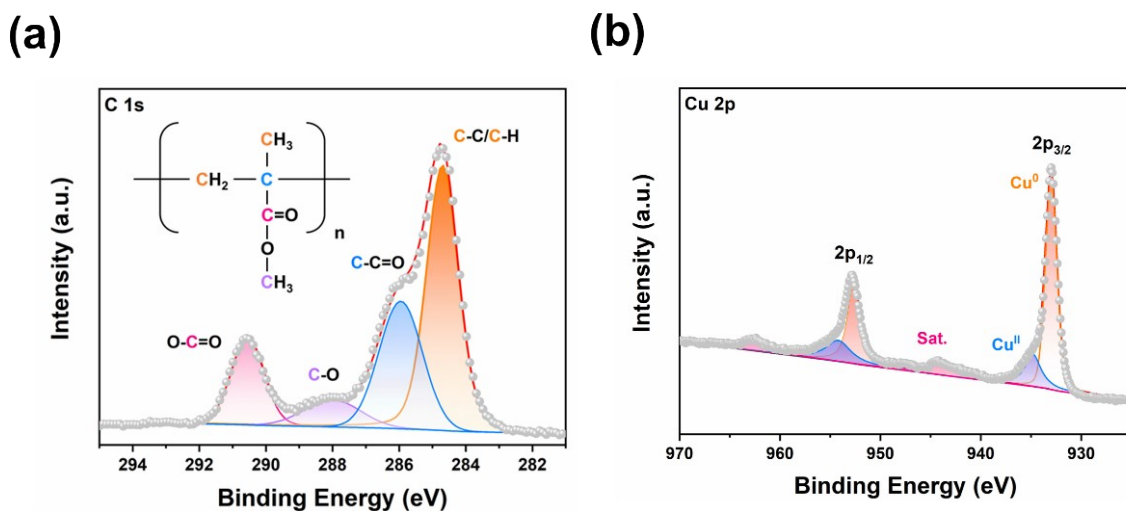


**Figure S7.** XPS spectrum for Cu@ 8%PMMA-MS. a) XPS C 1s spectra and b) XPS Cu 2p spectra.

To investigate the surface compositions and chemical states, high-resolution C 1s X-ray photoelectron spectroscopy (XPS) spectrum of Cu@PMMA 8%-MS (Figure S7a) could be well fitted into four peaks at the binding energy of 284.8, 285.98, 288.08 and 290.58 eV, corresponding to C–C/C–H, C–C=O, C–O and O–C=O in PMMA, respectively.<sup>5</sup> As expected, the high-resolution Cu 2p XPS spectrum (Figure S7b) reveals that the Cu element are mainly composed of Cu<sup>0</sup> (933 eV), with a small fraction of oxidized Cu<sup>II</sup> (934.88 eV).

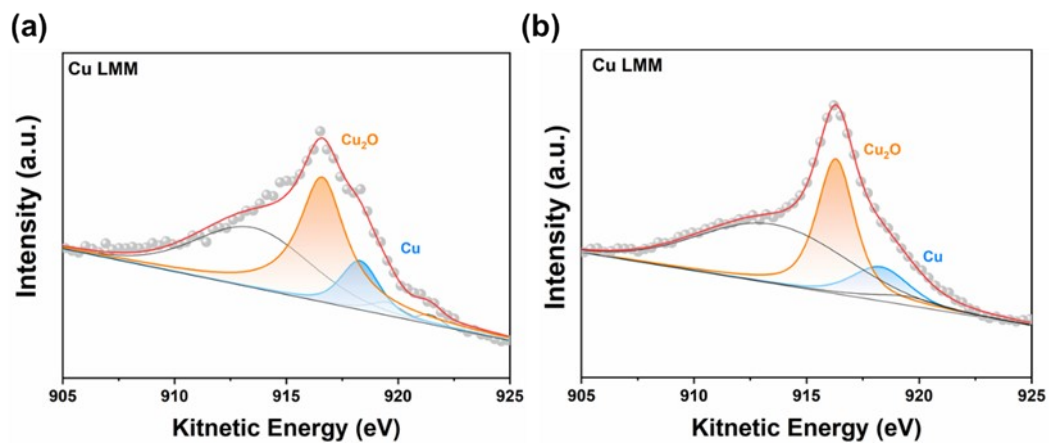


**Figure S8.** Cu Auger LMM spectra for (a) Commercial Cu and (b) Cu@8% PMMA-MS.

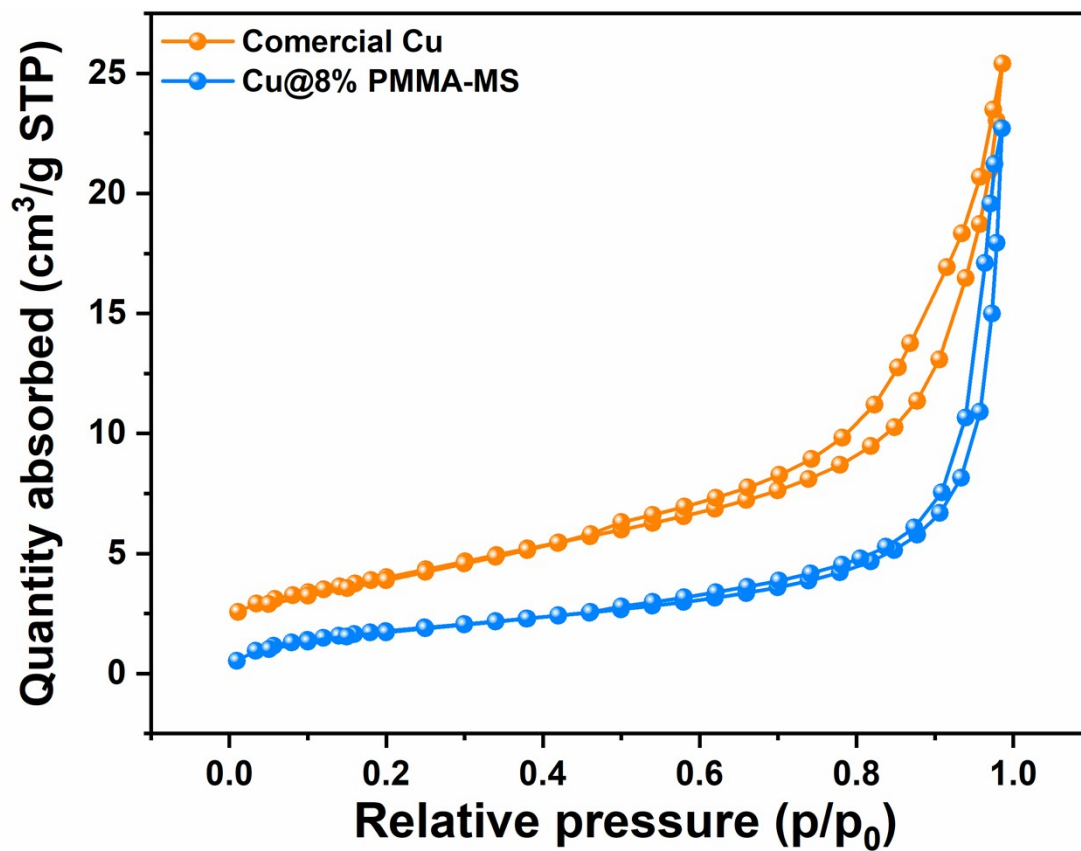
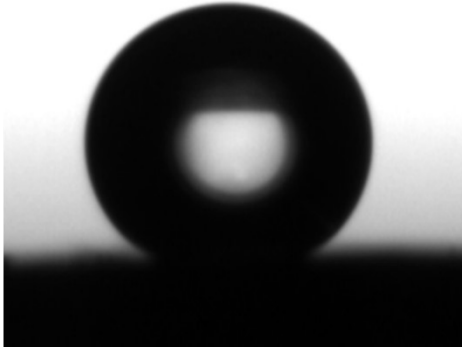
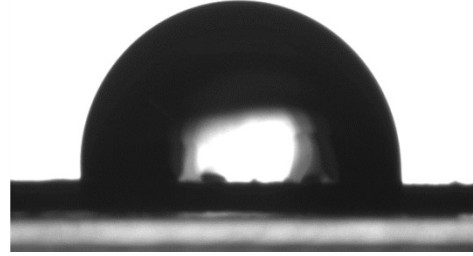


Figure S9. N<sub>2</sub> adsorption–desorption isotherm for Cu@8% PMMA-MS and commercial Cu.

**(a)**



**(b)**



**Figure S10** Water contact angle for a) GDL (SGL 28BC) substrate and b) commercial Cu.

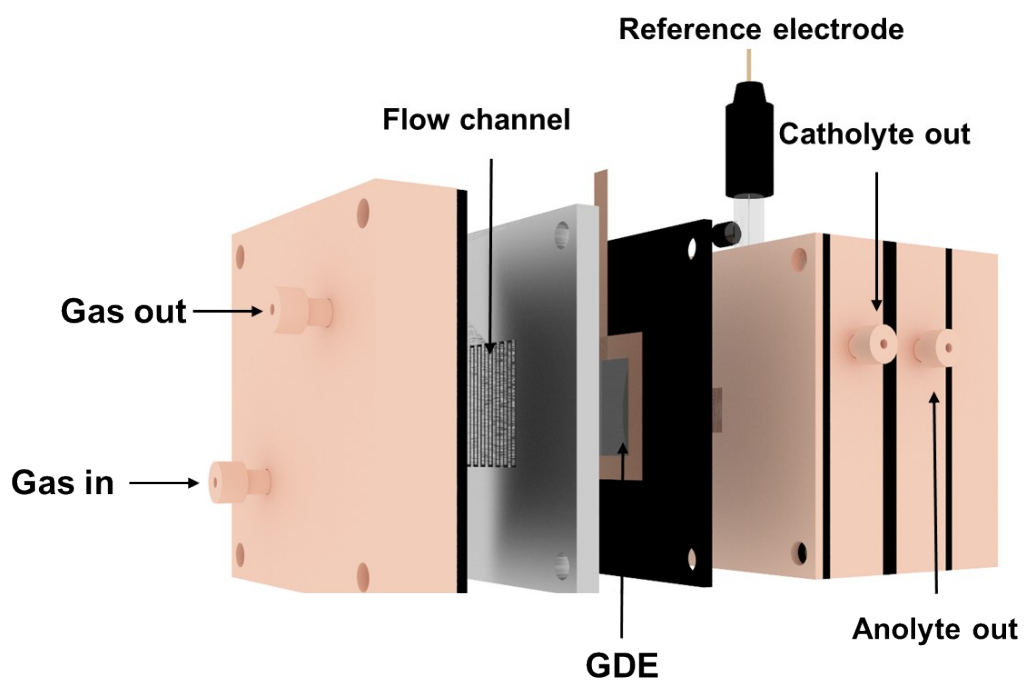


**Figure S11.** Schematic demonstration for flow cell used for ECORR.

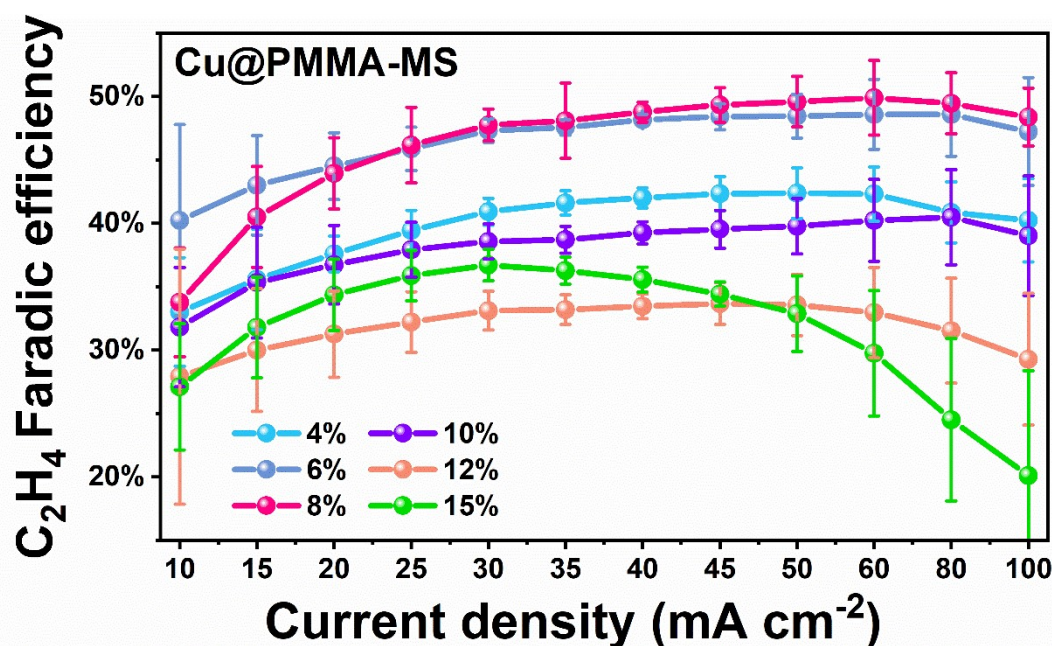


**Figure S12.** Current density-dependent C<sub>2</sub>H<sub>4</sub> Faradic efficiency of Cu@X%PMMA-MS (X=4, 6, 8, 10, 12 and 15).

Cu@PMMA-MS prepared from dispersions with a PMMA concentration of 4%, 6%, 8%, 10%, 12% and 15% were tested under various current densities, corresponding to the C<sub>2</sub>H<sub>4</sub> faradic efficiency of 42.4%, 48.6%, 49.9%, 40.5%, 33.6%, and 36.7%, respectively. Among these concentrations, Cu@8%PMMA-MS exhibits the maximum faradic efficiency of 49.9% at the current density of 60 mA cm<sup>-2</sup>, nearly no attenuation is observed with current density increase from 60 to 80 mA cm<sup>-2</sup>, and only a slightly decrease appeared with current density further increase to 100 mA cm<sup>-2</sup>.

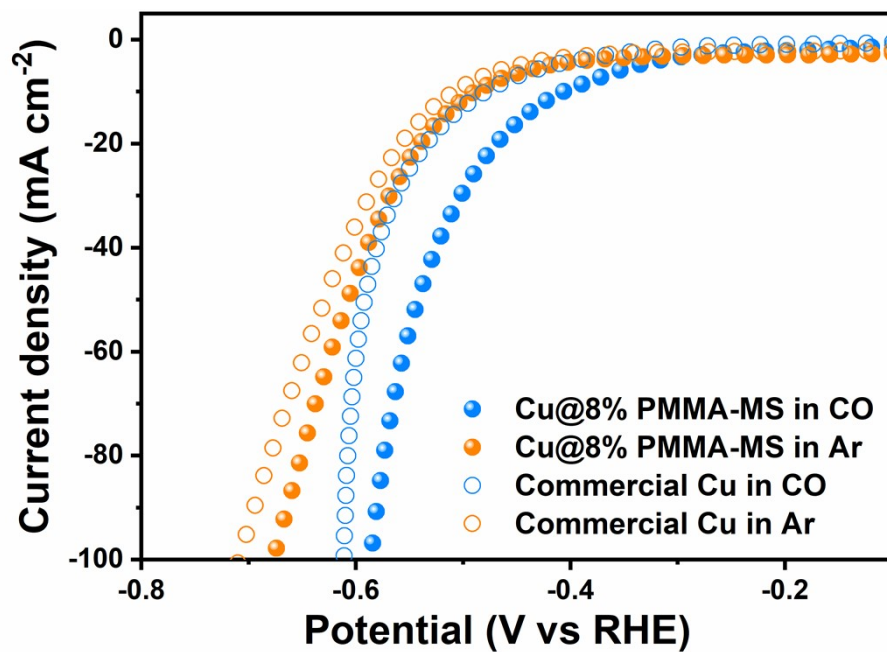


**Figure S13.** Linear sweep voltammetry curves for Commercial Cu and Cu@8%PMMA-MS in Ar and CO.

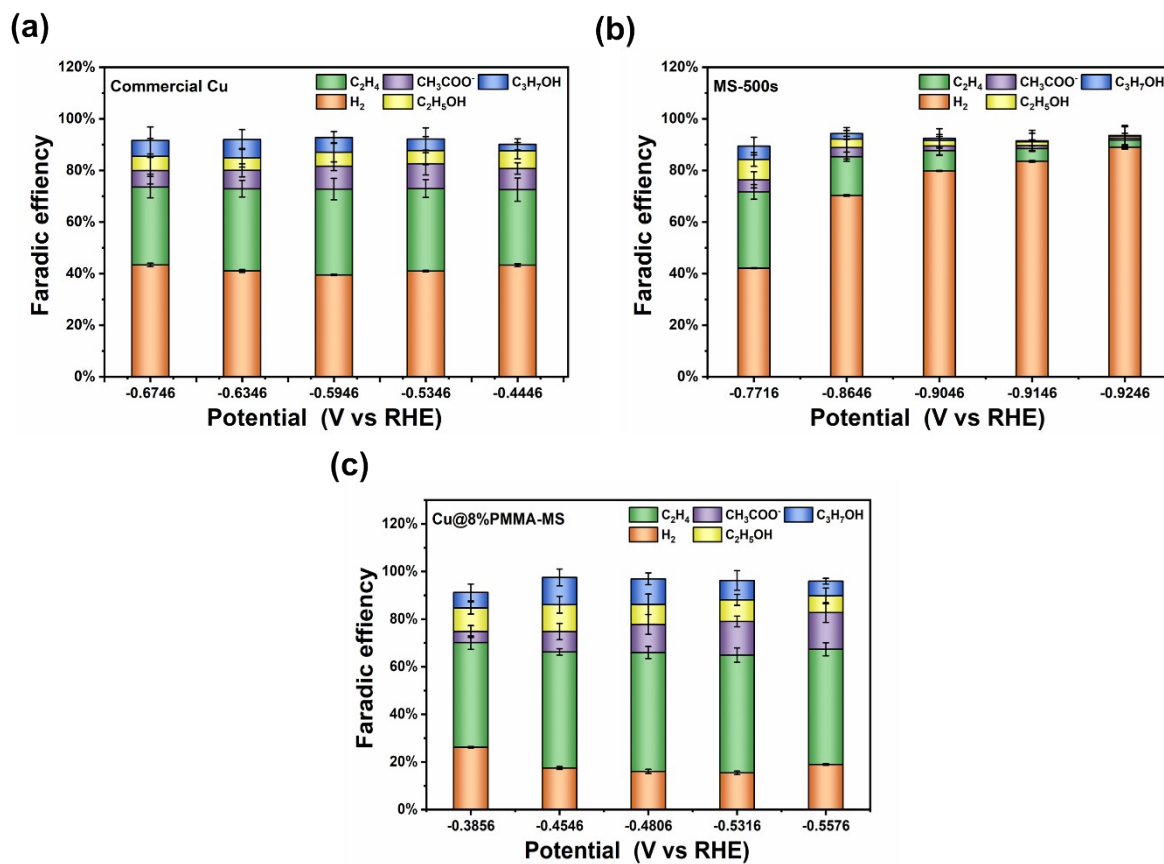


**Figure S14** Products distribution for commercial Cu, MS-500s and Cu@8% PMMA-MS during ECORR.

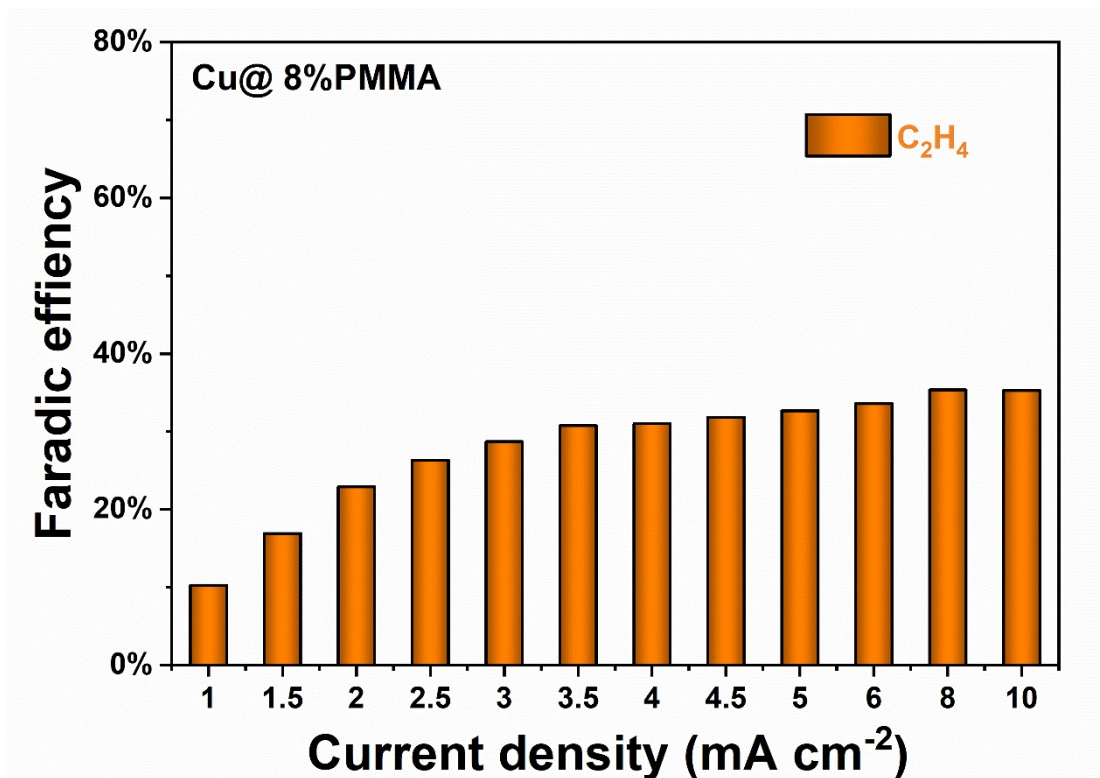
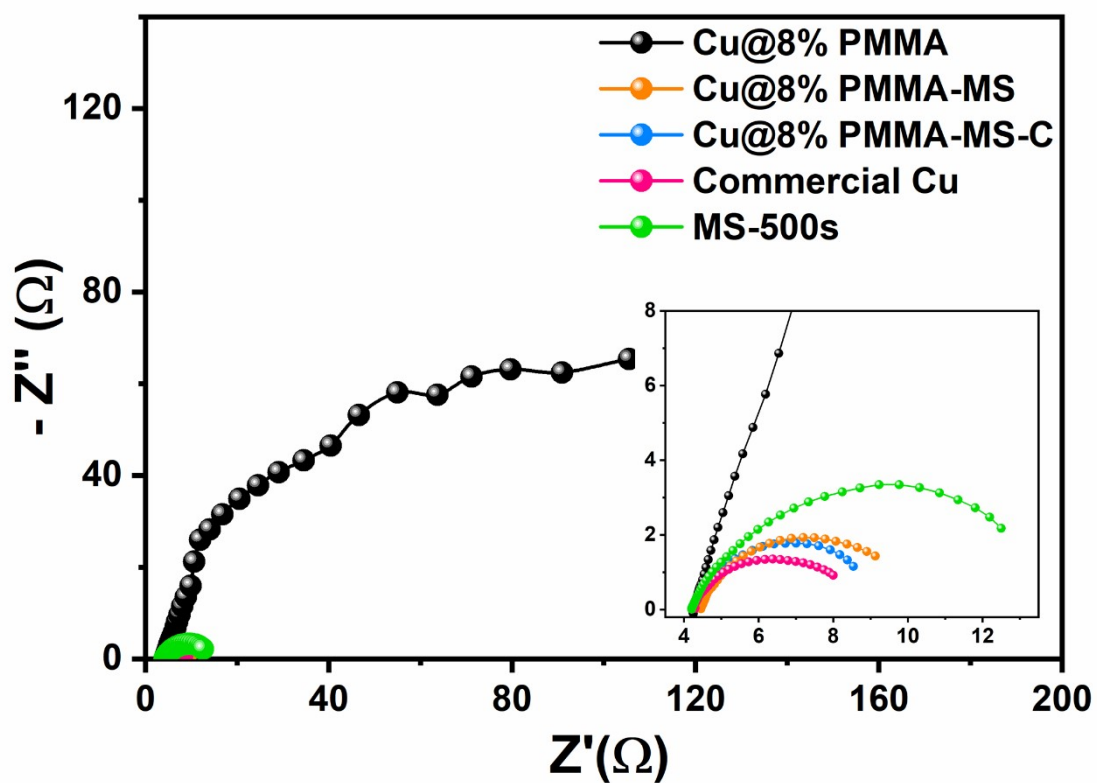


Figure S15. Current density-dependent C<sub>2</sub>H<sub>4</sub> Faradic efficiency of Cu@8%PMMA.



**Figure S16.** EIS of commercial Cu, Cu@8%PMMA Cu@8%PMMA-MS, MS-500s and Cu@8%PMMA-MS/C tested at -0.6 V vs RHE.

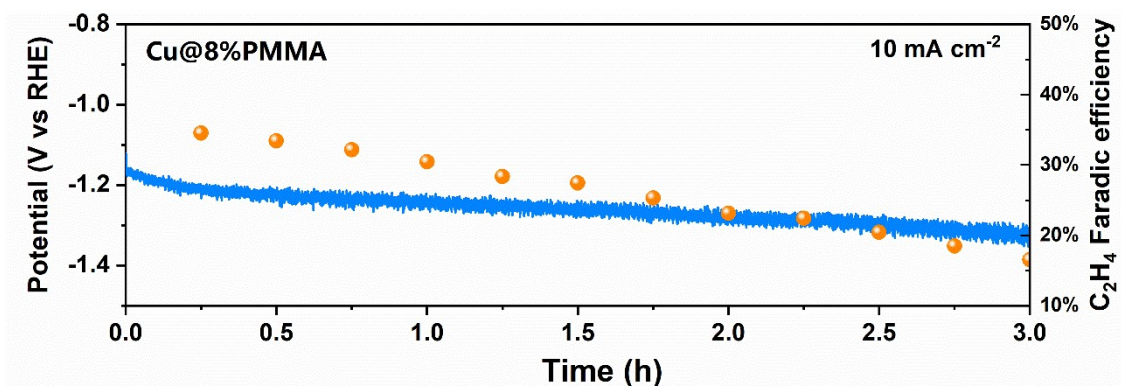
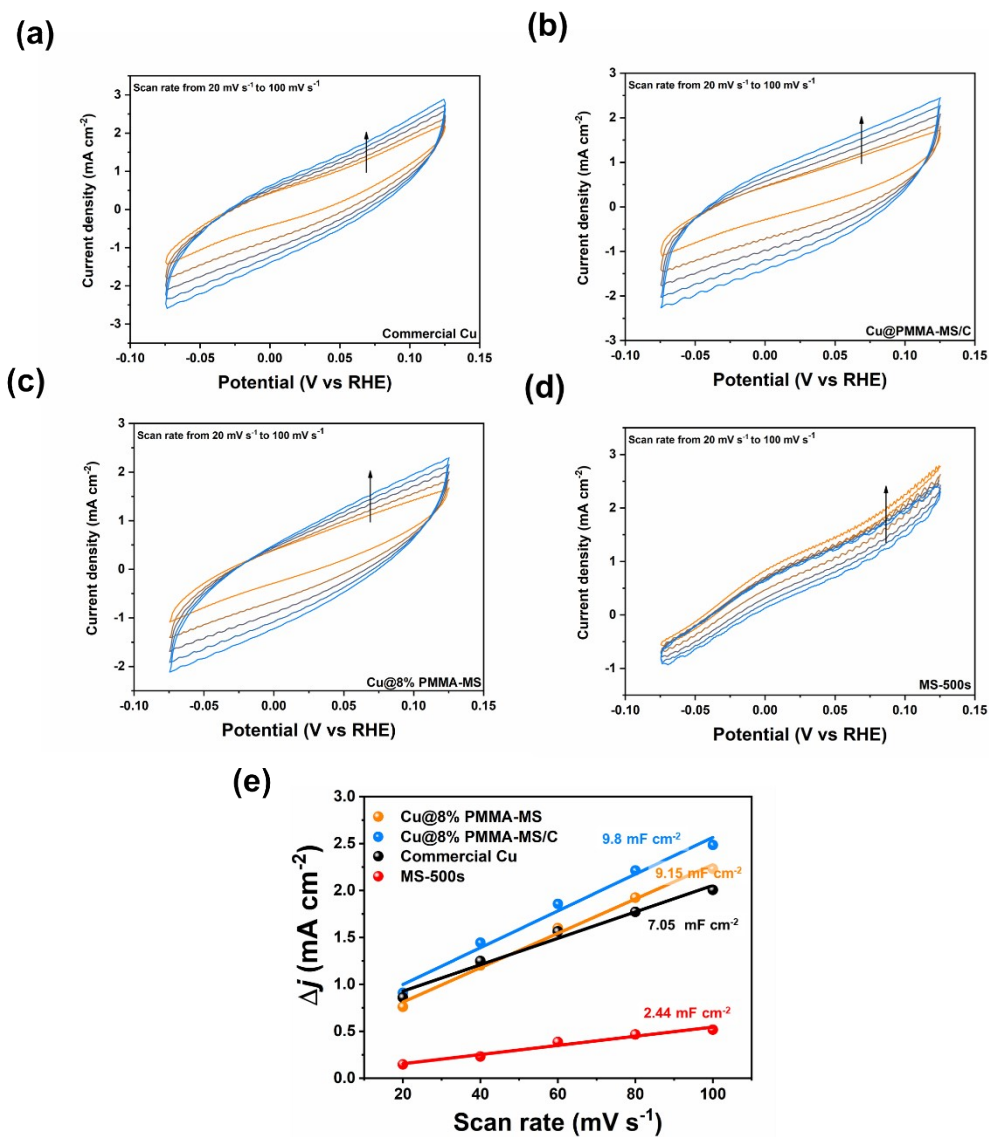
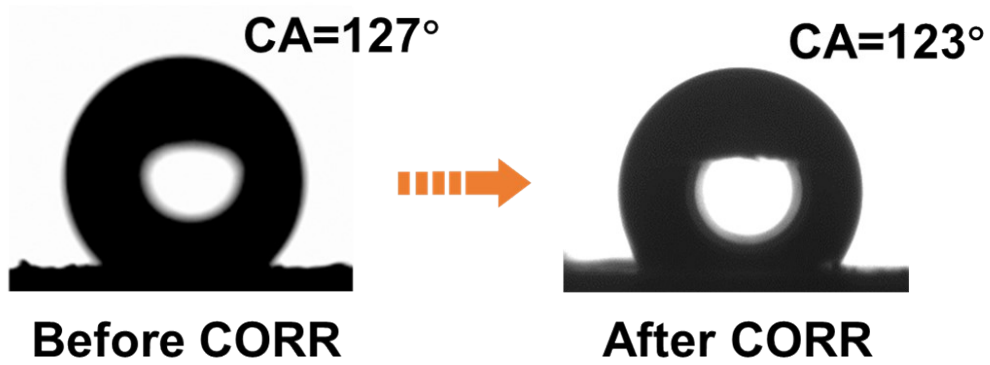


Figure S17 Galvanostatic stability tests for Cu@8%PMMA at 10 mA cm<sup>-2</sup>



**Figure S18.** CV scans measured in a narrow potential window where only double-layer charging and discharging occur at various scan rates for a) commercial Cu, b) Cu@8%PMMA-MS/C, c) Cu@8%PMMA-MS and d) MS-500. e) Charging current density differences plotted against scan rates for the four samples. The fitting slopes are twice that of the  $C_{dl}$  values.

**Cu@ 8%PMMA-MS**



**Commercial Cu**

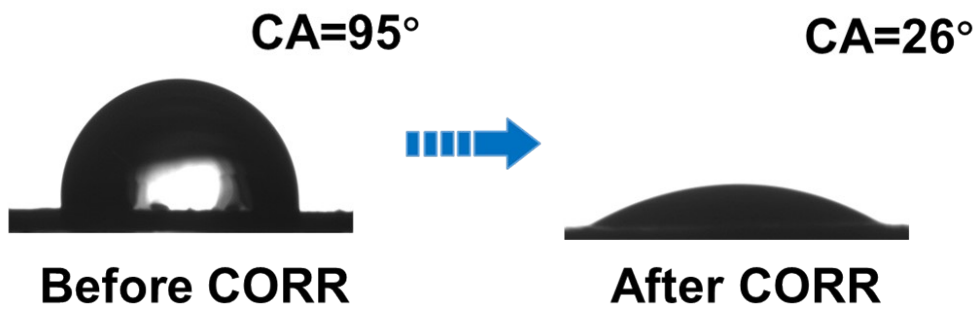


**Figure S19.** CAs for Cu@8%PMMA-MS and commercial Cu before and after 3h ECORR.

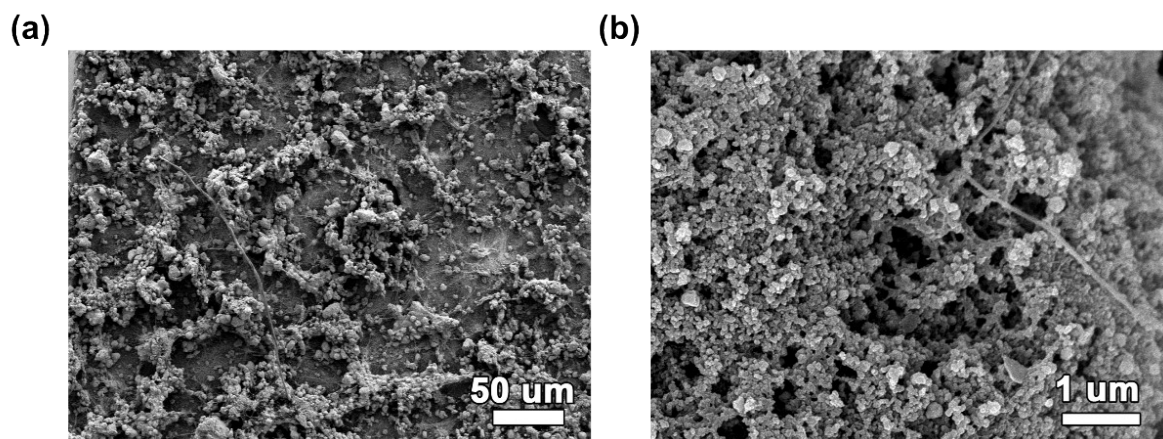


**Figure S20.** The SEM images of Cu@8%PMMA-MS after 3h-ECORR test under 100 mA  $\text{cm}^{-2}$ . The scale bars are a) 50  $\mu\text{m}$  and b) 1  $\mu\text{m}$ , respectively.

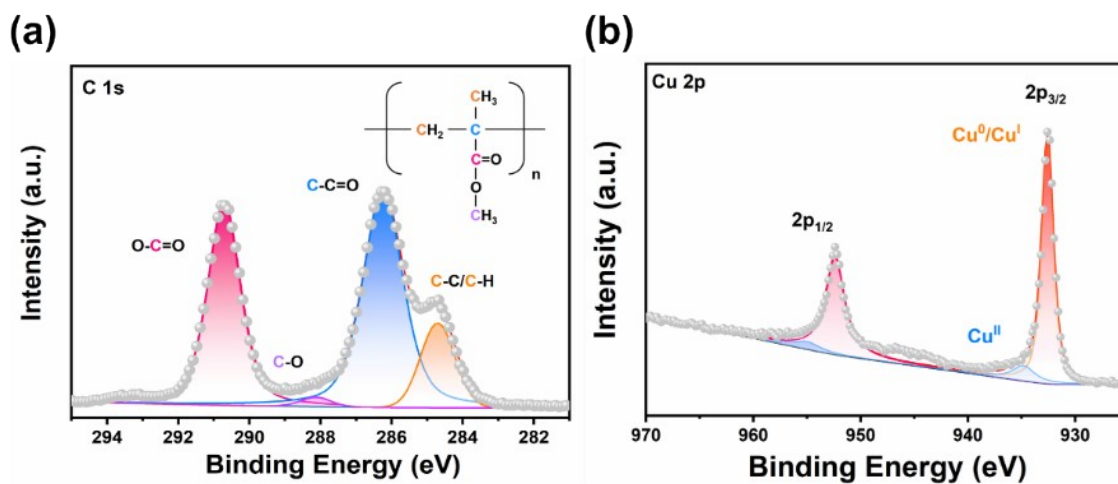


**Figure S21.** XPS spectrum for Cu@ 8%PMMA-MS after ECORR test. a) XPS C 1s spectra and b) XPS Cu 2p spectra.

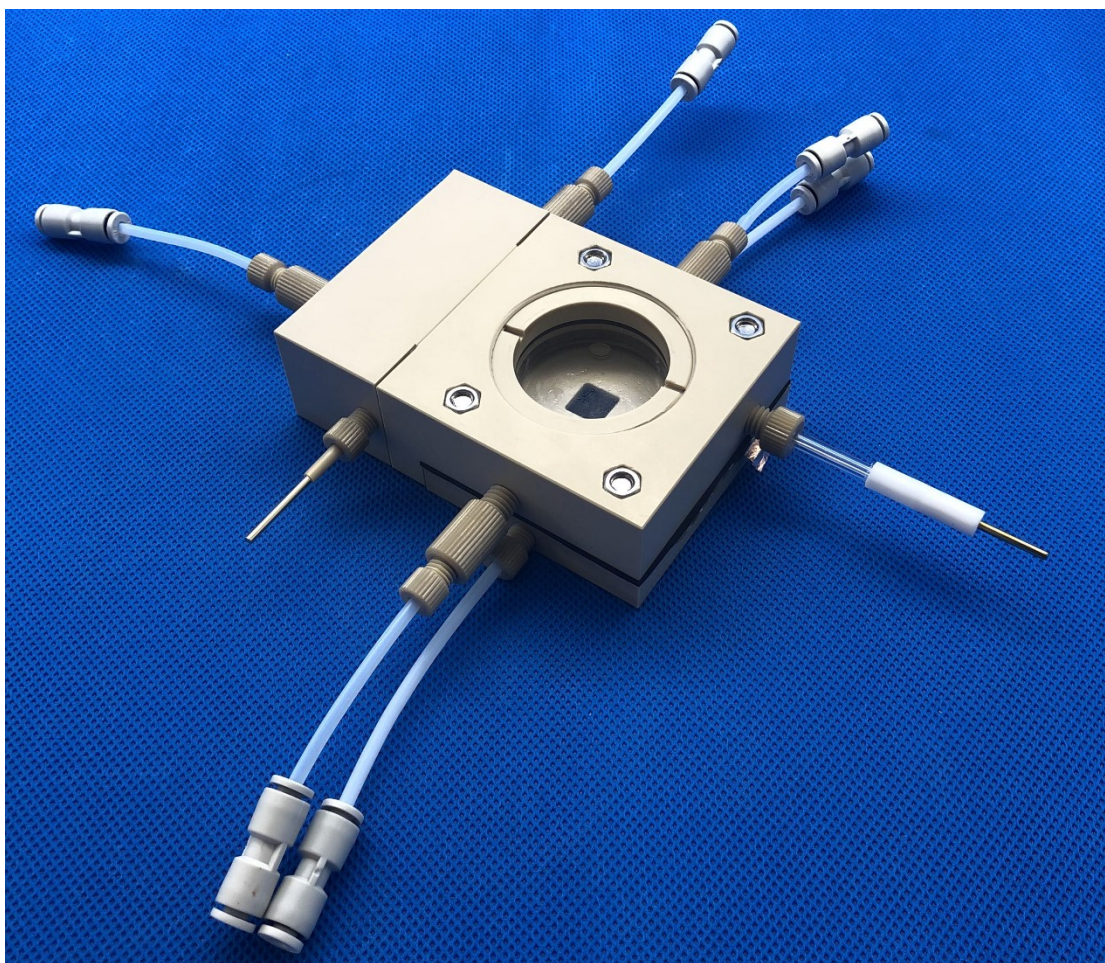


**Figure S22.** Digital photograph of flow cell with optical window used for *in situ* Raman measurement.

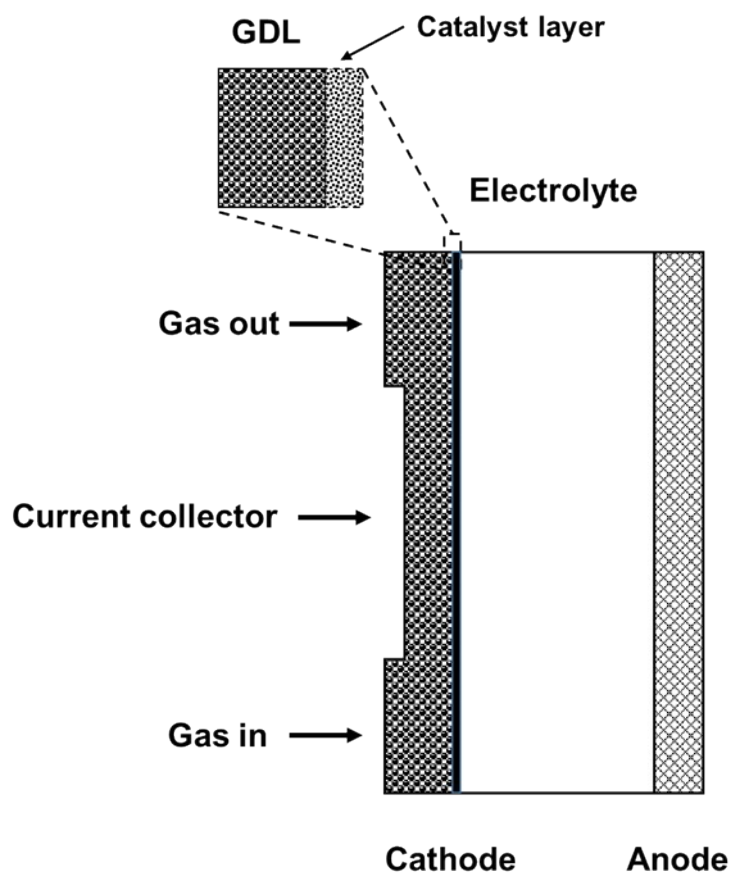


**Figure S23.** The geometry model of flow cell in 2D dimension domain.

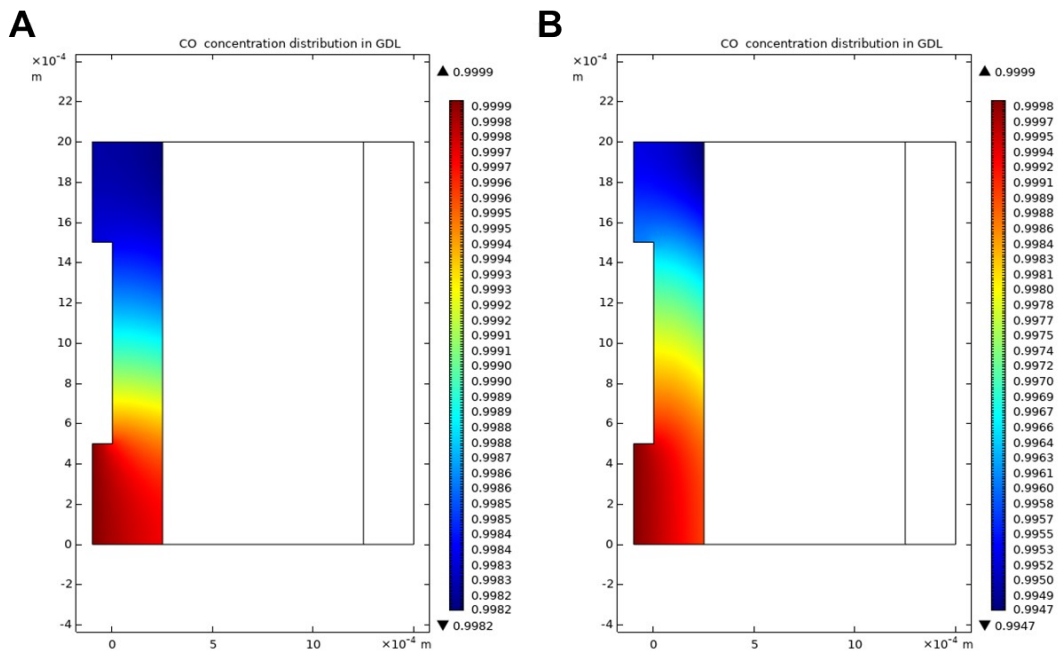


**Figure S24.** The modeling investigation of CO concentration distribution in GDL using COMSOL 5.4. The porosity is a) 20% and b) 80%, respectively.

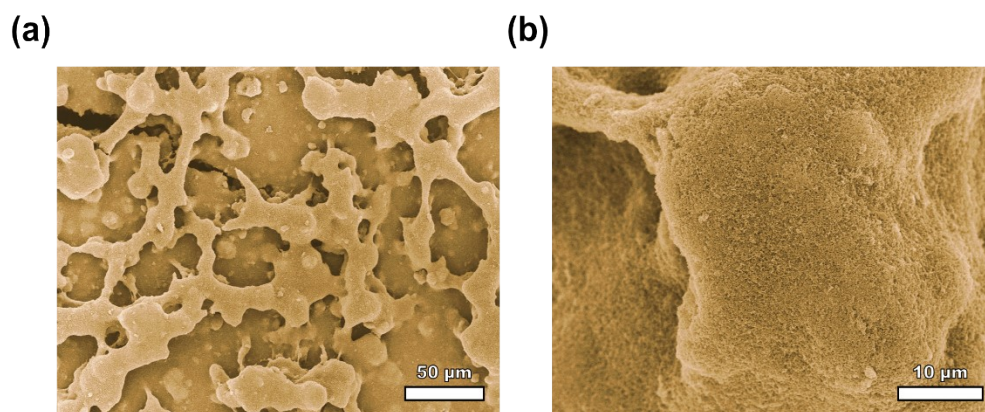


**Figure S25.** SEM images of Kenjen black covered Cu@8% PMMA-MS (Cu@8% PMMA-MS/C). The scale bars are a) 50 μm and b) 10 μm, respectively.

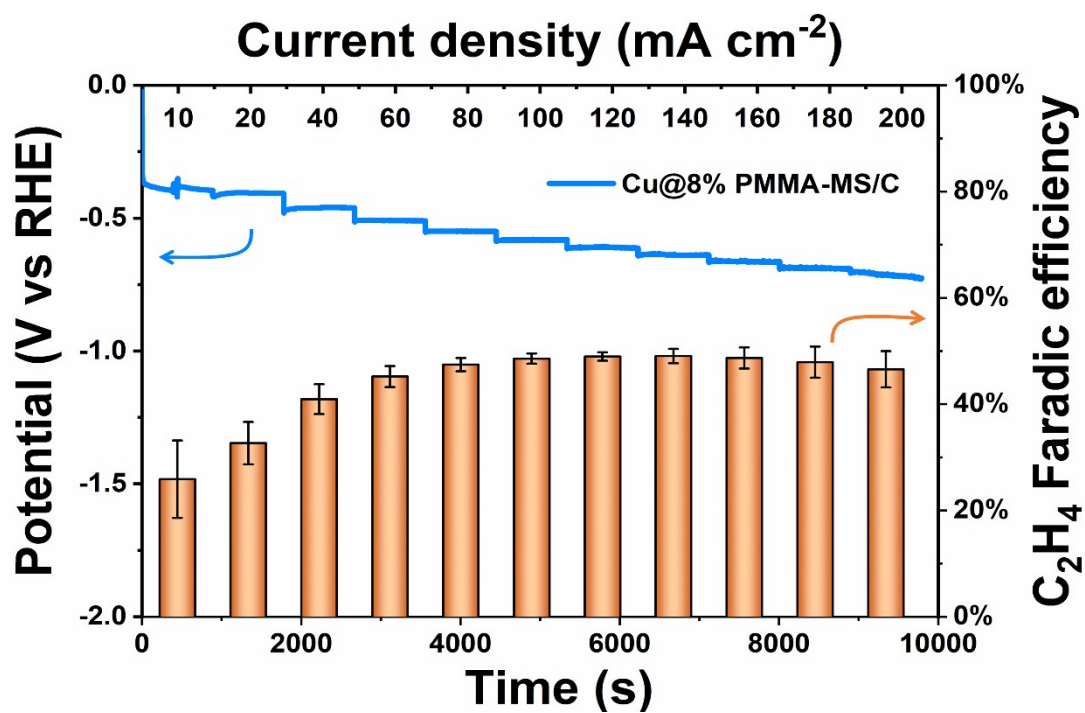


**Figure S26.** Current density-dependent potentials (upper blue line) and C<sub>2</sub>H<sub>4</sub> Faradic efficiency (bar graph below) of Cu@8%PMMA-MS/C.

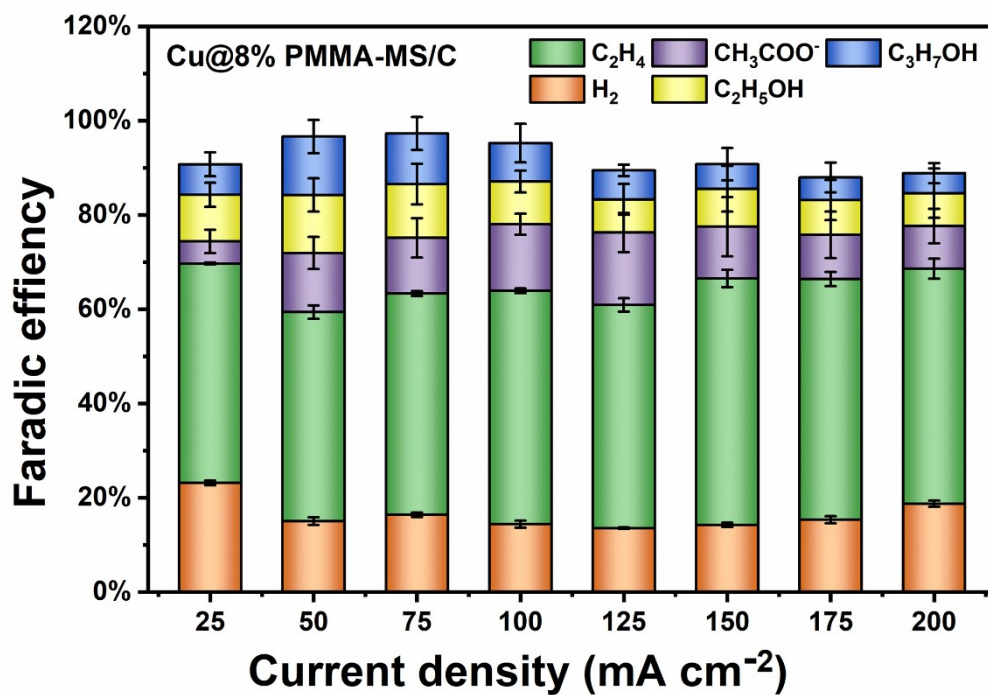


**Figure S27.** Total products distribution of Cu@8%PMMA-MS/C under various current densities.

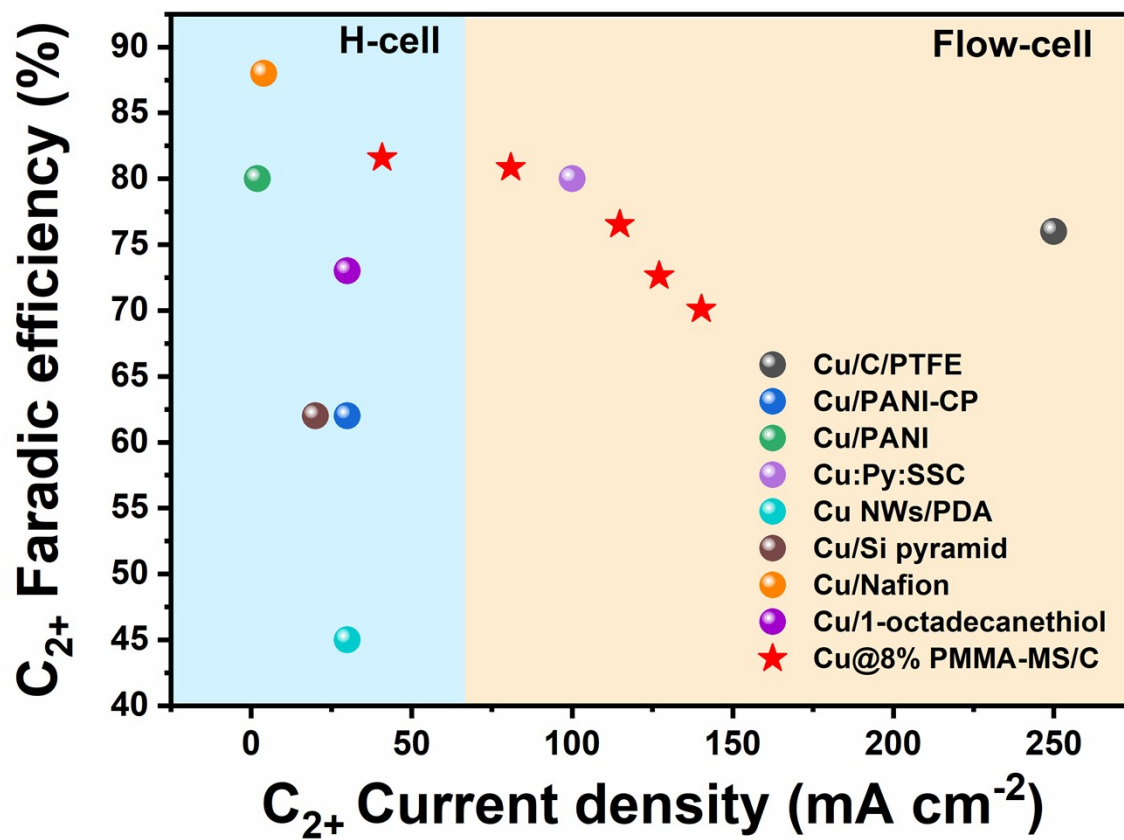


**Figure S28.** Comparison of C<sub>2+</sub> current densities and C<sub>2+</sub> FEs (see Table S2 for details) for various copper hybrid electrodes reported in the literature.

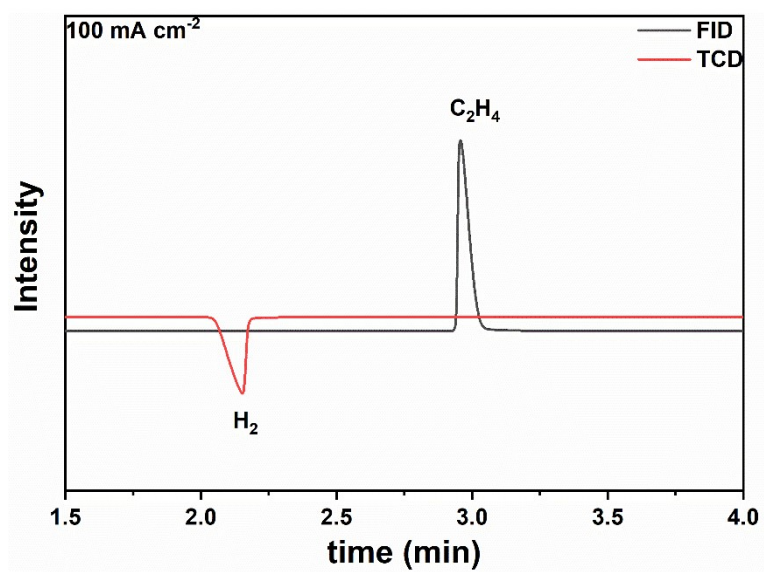


**Figure S29** GC traces for Cu@8%PMMA-MS/C gas product at 100 mA cm<sup>-2</sup>.

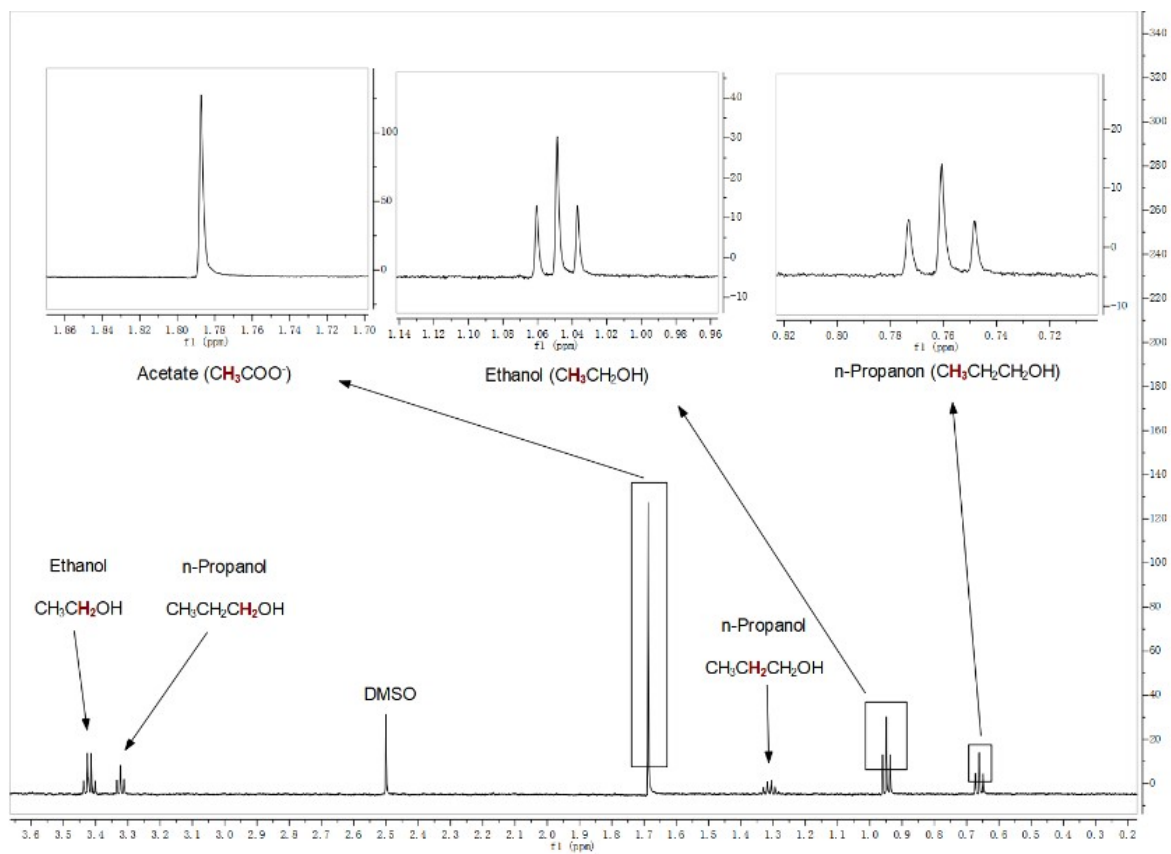


**Figure S30** NMR analysis for  $\text{Cu}@8\%\text{PMMA-MS/C}$  liquid product at  $100 \text{ mA cm}^{-2}$ .

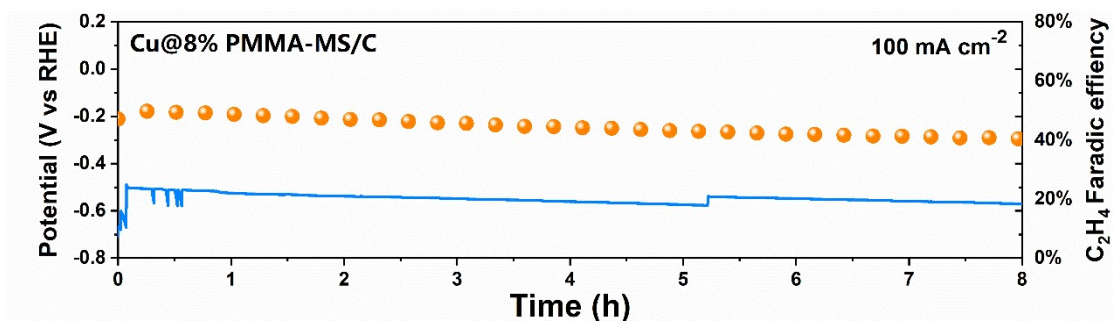


**Figure S31** Galvanostatic stability tests for Cu@8%PMMA-MS/C at 100 mA cm<sup>-2</sup>, chronopotentiometry curves on the top and Faradic efficiencies at the bottom.

**Table S1.** Summary of Cu LMM Peaks Fitting with relative intensity.

Sample	Species	Kinetic Energy (eV)	Intensity (a.u.)
Commercial Cu	Cu	916.3	11885
	Cu <sub>2</sub> O	918.3	19225
Cu@8% PMMA- MS	Cu	926.4	7797
	Cu <sub>2</sub> O	918.3	22497

**Table S2** Summary of Catalyst mass loading for Cu@X% PMMA and Cu@X%PMMA-MS.

Mass loading (mg cm <sup>-2</sup> )	X=4	X=6	X=8	X=10	X=12	X=15
Cu@X%PMMA	0.693	0.664	0.683	0.669	0.652	0.645
Cu@X%PMMA-MS	0.693	0.665	0.683	0.669	0.653	0.645

**Table S3** EDS result for Cu@8% PMMA

<b>Element</b>	<b>Weight (wt.%)</b>	<b>Atom(at. %)</b>
O K	34.84	35.81
C K	14.85	31.89
Cu K	50.31	32.31
total	100.00	100.00

**Table S4**  $R_{ct}$  for the samples.

<b>Commercial</b>	<b>Cu@8%</b>	<b>Cu@8%</b>	<b>Cu@8%</b>	<b>MS-500s</b>
<b>Cu</b>	<b>PMMA</b>	<b>PMMA-MS</b>	<b>PMMA-MS-C</b>	
4.3 $\Omega$	~200 $\Omega$	6 $\Omega$	4.8 $\Omega$	10.5 $\Omega$

**Table S5** Comparison of C<sub>2+</sub> FEs and C<sub>2+</sub> partial current densities for various copper hybrid electrodes reported in the literature.

<b>Electrolyze r</b>	<b>Catalyst</b>	<b>C<sub>2+</sub> FE (%)</b>	<b>C<sub>2+</sub> current density (mA cm<sup>-2</sup>)</b>	<b>Ref</b>
H-cell	Cu/PANI-CP	62	30	26
	Cu/1-octadecanethiol	73	30	31
	Cu/Nafion	88	30	41
	Cu/PANI	80	~1	42
	Cu/Si pyramid	62	20	43
	Cu NWs/PDA	~45	30	44
Flow-cell	Cu/C/PTFE	76	250	25
	Cu:Py:SSC	80	100	37
	Cu@ 8%PMMA- MS/C	81.6	40.8	This work
	Cu@ 8%PMMA- MS/C	80.8	80.8	This work
	Cu@ 8%PMMA- MS/C	76.5	114.8	This work
	Cu@ 8%PMMA- MS/C	72.6	127.1	This work
	Cu@ 8%PMMA- MS/C	70.1	140.2	This work

## Reference

- (1) Li, J.; Chang, X.; Zhang, H.; Malkani, A. S.; Cheng, M.-j.; Xu, B.; Lu, Q. *Nat. Commun.* **2021**, *12*, 1-11.
- (2) Dinh, C.-T.; Burdyny, T.; Kibria, M. G.; Seifitokaldani, A.; Gabardo, C. M.; De Arquer, F. P. G.; Kiani, A.; Edwards, J. P.; De Luna, P.; Bushuyev, O. S. *Science* **2018**, *360*, 783-787.
- (3) Xing, Z.; Hu, L.; Ripatti, D. S.; Hu, X.; Feng, X. *Nat. Commun.* **2021**, *12*, 1-11.
- (4) Ramesh, S.; Leen, K. H.; Kumutha, K.; Arof, A. *Spectrochim. Acta A* **2007**, *66*, 1237-1242.
- (5) Paul Pijpers, A.; Meier, R. *Chem. Soc. Rev.* **1999**, *28*, 233-238.